ELSEVIER

Materials Science and Engineering A261 (1999) 44–52

MATERIALS SCIENCE & ENGINEERING A

Mo_5Si_3 single crystals: physical properties and mechanical behavior

F. Chu *, D.J. Thoma, K.J. McClellan, P. Peralta

Materials Science and Technology Division, MS G755, Los Alamos National Laboratory, Los Alamos NM 87545, USA

Abstract

The materials processing, physical properties and mechanical behavior of an ultrahigh temperature structural silicide, Mo_5Si_3, have been studied. High purity single crystals of Mo_5Si_3 have been synthesized by both optical floating zone and Czochralski methods. The thermal and elastic properties of the Mo_5Si_3 single crystals were experimentally measured. Results show that Mo_5Si_3 has significant thermal expansion anisotropy along the a and c directions with $\alpha_c/\alpha_a = 2.2$. The single crystal elastic moduli of Mo_5Si_3 indicate that it has less elastic anisotropy and lower shear moduli than transition metal disilicides. Tensile stresses of up to 1.8 GPa can develop at grain boundaries after cooling from the melting point due to the thermal expansion mismatch in Mo_5Si_3, causing grain boundary cracking during processing of polycrystals. Room temperature Vickers indentation tests on (100) and (001) planes have been performed with different indenter diagonal orientations and the orientation dependence of hardness and fracture toughness of Mo_5Si_3 single crystals have been obtained. The corresponding deformation and fracture modes have been revealed by microscopy studies. Finally, a comparison of Mo_5Si_3 with other high temperature structural silicides is discussed.

Keywords: Structural silicide; Physical properties; Anisotropy; Fracture

1. Introduction

Many intermetalllics and silicides offer the desired properties for high temperature structural applications, e.g. a high melting point, high strength, good oxidation resistance, and excellent creep behavior at elevated temperatures. Some candidates have been studied extensively, e.g. nickel aluminides, titanium aluminides, and transition metal disilicides. Among these phases, refractory metal silicides appear to be more attractive because of their ultra-high melting temperatures [1]. Among the refractory metal silicides, the silicides in the Mo–Si system show promising potential because Mo has a lower density compared to other refractory metals, and Mo does not embrittle with oxygen and nitrogen contamination. In the Mo–Si system, there are three compounds, i.e. $C11_b$-structured $MoSi_2$, D_{8m}-structured Mo_5Si_3, and A15-structured Mo_3Si [2]. $MoSi_2$, along with some transition metal disilicides, has been studied extensively [1,3–8]. Mo_5Si_3 and Mo_3Si are receiving more attention recently in studies of their physical properties and mechanical behavior [9–11].

Mo_5Si_3 belongs to the space group $I4/mcm$ (140). As a body-cantered tetragonal lattice (tI32), it has 20-Mo atoms and 12-Si atoms in the unit cell. Mo_5Si_3 has the following structural characteristics [11]: (1) its a-lattice parameter is larger than its c-lattice parameter ($a/c \approx 2$), which is different from typical tetragonal high temperature structural silicides, e.g. $MoSi_2$; (2) it has no close-packed planes, which is also different from other tetragonal silicides, e.g. $MoSi_2$; and (3) the–Si–Mo–Si– chains in Mo_5Si_3 are along [100] and [010] directions (these chains may also be along other directions, e.g. <331]) and the –Mo–Mo– and –Si–Si– chains are along [001] direction. On the other hand, the –Si–Mo–Si– chains in $MoSi_2$ are along [001] direction and the –Mo–Mo– and –Si–Si– chains are along the [100] and [010] directions. It is generally true that the interatomic bonding strength of the –Si–Mo–Si– chains is stronger than those of the –Mo–Mo– and –Si–Si– chains. Mo_5Si_3 has a very high melting point of 2180°C [2], which is substantially higher than that of $MoSi_2$ (2020°C) and a reasonable density of 8.19 g cm^{-3}, which is higher than that of $MoSi_2$ (6.3 g cm^{-3}). Therefore, it is considered as a promising ultra-high temperature structural material. In addition, Mo_5Si_3 has a relatively large range of nonstoichiometry (2–3

* Corresponding author..

0921-5093/99/$ - see front matter
PII: S0921-5093(98)01048-X

Table 1
Chemical analysis results of the Mo_5Si_3 alloys (from [11])

	Mo (at.%)	Si (at.%)	O (wppm)	N (wppm)
Starting elementals	62.50	37.50		
Polycrystalline Mo_5Si_3	62.75	37.25	20	10
Single crystal Mo_5Si_3	62.92	37.08	10	10

at.%), compared to $MoSi_2$ which is basically a line compound, according to the Mo–Si phase diagram [2].

Initial studies for the fundamental physical properties and mechanical behavior of Mo_5Si_3 single crystals have been performed. In this proceedings, we report based on the previously published results [11]: (a) the synthesis of high-quality single crystals; (b) the measurement of physical properties; (c) the calculation of residual thermal stresses; and (d) the mechanical behavior of Mo_5Si_3 single crystals.

2. Experimental procedures and calculation methods

2.1. Synthesis of the Mo_5Si_3 single crystals

Elemental Mo and Si with nominal purities of 99.97 and 99.95 at.% were chemically cleaned before alloying. Mo_5Si_3 alloys were made in the form of buttons and rods by arc-melting. Single crystals of Mo_5Si_3 were grown by the optical floating zone technique using arc-melted rods and by the Czochralski method using a tri-arc crystal growth furnace and arc-melted buttons [11].

Chemical analysis was conducted for both the as-melted polycrystals and the asgrown single crystals of Mo_5Si_3. In this analysis, the Mo and Si contents were analyzed by direct current plasma emission spectroscopy. The oxygen and nitrogen contents were characterized by inert gas fusion experiments.

2.2. Measurement of the physical properties of Mo_5Si_3

Using the Mo_5Si_3 single crystals, the thermal and elastic properties of Mo_5Si_3 were measured [11]. In the thermal property investigation, the thermal expansion of single crystal Mo_5Si_3 was examined using a Perkin-Elmer DMA-7 thermal-mechanical analyzer (TMA) operated in TMA mode in the regime 298–773 K. The coefficients of thermal expansion (CTE) along the a and c axes were measured on a rectangular parallelepiped specimen (5 mm [100] × 5 mm [010] × 4 mm [001]), which was cut using a diamond wafer blade from the as-grown single crystals after orienting it using the Laue back reflection technique and polished using SiC papers and diamond lapping films. The CTE along the a axis was obtained from the measurement along the larger dimension (5 mm) and the CTE along the c axis was obtained from the measurement along the shorter dimension (4 mm).

Table 2
The thermal expansion data of Mo_5Si_3 and $MoSi_2$

Materials	α_a (10^{-6} °C^{-1})	α_c (10^{-6} °C^{-1})	β (10^{-6} °C^{-1})	α_c/α_a
Mo_5Si_3	5.2	11.5	21.9	2.21
$MoSi_2$	8.2	9.4	25.8	1.15

Resonant ultrasound spectroscopy (RUS) was employed to measure the room temperature single crystal elastic moduli of Mo_5Si_3. The single crystal Mo_5Si_3 specimen was cut and polished, as described above, into a rectangular parallelepiped geometry with dimensions $x_1 = 3.217 \pm 0.002$ mm, $x_2 = 2.950 \pm 0.001$ mm, and $x_3 = 3.702 \pm 0.003$ mm. The Laue back reflection X-ray technique was used to orient x_1 parallel to [100], x_2 parallel to [010] and x_3 parallel to [001]. The mass density of the specimen was determined from its dimensions and mass. The room temperature single crystal elastic moduli were determined using 70 resonant frequencies from 0.45–1.82 MHz.

2.3. Calculation of the residual thermal stresses in Mo_5Si_3

Using the coefficients of thermal expansion and elastic moduli of single crystal Mo_5Si_3, the residual thermal stresses developed in the solidification process are calculated for two cases. One is for a single spherical grain of Mo_5Si_3 embedded in an infinite Mo_5Si_3 matrix using the stress associated with the elastic fields of spherical inclusions in anisotropic solids [12,13]. The other is for two grains of Mo_5Si_3, assuming that the interfaces can be modelled as the boundaries between two semi-infinite anisotropic solids [14].

2.4. Characterization of the mechanical behavior of Mo_5Si_3

Room temperature Vickers indentation tests were performed on the (100) and (001) planes of Mo_5Si_3 single crystals with different orientations of the indenter diagonal using a Micromet 4 microhardness tester. The applied load was 1 kg for 10 s. For each orientation of the indenter diagonal on each plane, five indents were made and the average values of the indentation impression and crack length measurements were obtained from the five indents. Using these averaged values, the Vickers hardness of Mo_5Si_3 single crystals along an orientation on a specific plane was calculated using [15]:

Table 3
Room temperature elastic stiffness and compliance constants of Mo_5Si_3 single crystals (from [11])

(i, j)	11	33	13	12	44	66
c_{ij} (GPa)	446	390	140	174	110	140
s_{ij} (10^{-3} GPa^{-1})	2.80	3.06	−0.69	−0.87	9.09	7.14

$$H = 1.8544 \frac{P}{d^2} \quad (1)$$

where P is the load along the orientation on the plane the d is the impression diagonal average. The corresponding indentation fracture toughness of Mo_5Si_3 was roughly estimated from [15]:

$$K = 0.016 \left(\frac{E}{H}\right)^{1/2} \frac{P}{c^{3/2}} \quad (2)$$

where c is the radial crack length average. E and H are the Young's modulus and hardness for the corresponding orientation. The impressions and cracks of the indents were further characterized using a JEOL 6300 scanning electron microscope with a field emission gun.

3. Results and discussion

3.1. Single crystal fabrication

The examination using Laue back-reflection X-ray patterns for the as-grown Mo_5Si_3 crystals confirmed that they are indeed single crystals [11]. Chemical analysis results for Mo, Si, O, and N are tabulated in Table 1. Table 1 indicates that the polycrystalline Mo_5Si_3 experienced some silicon loss during arc-melting, and single crystal Mo_5Si_3 had further silicon loss during crystal growth because of the silicon evaporation in these processes. However, these losses are minimal, being less than 0.5 at.%, so that the compositions of the alloys are still in the single phase region according to the Mo–Si phase diagram [2]. Using the data shown in Table 1, excess silicon can be added prior to the alloying process in order to precisely control the stoichiometry of Mo_5Si_3. It can also be found from Table 1 that the O and N impurities are very low in both polycrystalline and single crystal Mo_5Si_3 alloys, indicating that the techniques can be successfully employed to synthesize high purity Mo_5Si_3 single crystals. Using these crystals, the physical properties and mechanical behavior of Mo_5Si_3 have been investigated.

3.2. Physical properties

Thermal expansion coefficients were obtained as a function of temperature along the $a = [100]$ and $c = [001]$ axes for Mo_5Si_3 single crystals [11]. These coefficients are essentially temperature independent over the measured temperature range. Linear curve fits of the experimental results yield the CTEs of $\alpha_a = 5.2 \times 10^{-6}$ °C^{-1} and $\alpha_c = 11.5 \times 10^{-6}$ °C^{-1} for Mo_5Si_3 single crystals. The coefficient of volume (bulk) expansion is $\beta = 2\alpha_a + \alpha_c = 21.9 \times 10^{-6}$ °C^{-1}. The most striking feature of the CTEs of Mo_5Si_3 single crystals is their strong thermal expansion anisotropy, i.e. $\alpha_c/\alpha_a = 2.2$, which is substantially different from those of high temperature structural disilicides. The data in Table 2 list the thermal expansion values for Mo_5Si_3 and $MoSi_2$. It is found from Table 2 that $MoSi_2$ is almost thermally isotropic, because its value of α_c/α_a is close to 1. Strong thermal expansion anisotropy ($\alpha_c/\alpha_a = 2.2$) of Mo_5Si_3 suggests that the crystal anharmonicity is higher along the c direction in Mo_5Si_3.

The room temperature RUS spectrum of Mo_5Si_3 single crystals shows high signal-to-noise ratio and high-Q resonant peaks [11], demonstrating the high quality of the specimen and the RUS measurement. A total of 70 RUS peaks in the regime 0.45–1.82 MHz were fitted and an r.m.s. error of 0.33% was obtained, indicating an excellent agreement between the experimentally measured and calculated RUS peaks. Therefore, the room temperature elastic parameters obtained from this study should be reliable.

Table 3 lists the single crystal elastic stiffness and compliance constants obtained from this study. Using these single crystal elastic parameters and formalism developed elsewhere [16,17], the orientation dependence of the Young's modulus of Mo_5Si_3 is plotted in Fig. 1. It was also found using these single crystal elastic parameters that: (a) the maximum Young's modulus of Mo_5Si_3 is along the [110] direction, $E_{max} = E_{[110]} = 364$ GPa; (b) the minimum Young's modulus of Mo_5Si_3 is along the [409] direction, $E_{min} = E_{[409]} = 294$ GPa; and (c) $E_{max}/E_{min} = 1.24$. Therefore, Mo_5Si_3 should be the stiffest along [110] and the most compliant along [409] in response to tension or compression loading within the elastic regime. Similarly, the orientation dependence of the shear modulus of Mo_5Si_3 is obtained and shown in Fig. 2. It can be seen from Fig. 2 that the lowest shear modulus is 110 GPa on the (001) plane along any direction, on the (100) plane along [001], and on the (110) plane along [001]. On the other hand, the shortest Burgers vector exists on the (100) plane along [001] and on the (110) plane along [001] in Mo_5Si_3, i.e. $b = [001]$. Therefore, it is reasonable to predict that the possible dislocation slip systems in Mo_5Si_3 are (100)/[001] and/or (110)/[001].

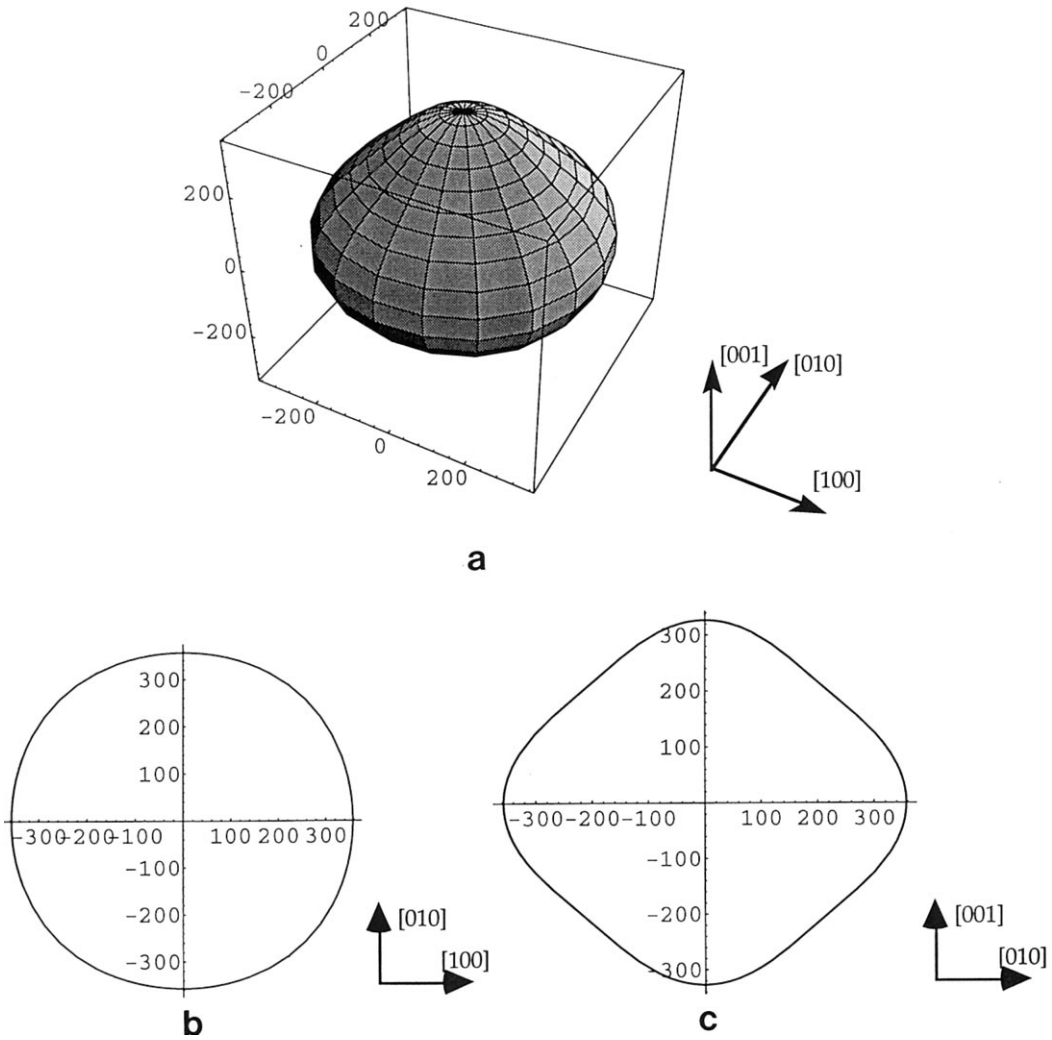

Fig. 1. The orientation dependence of the Young's modulus (in GPa) for Mo_5Si_3 single crystals: (a) 3-dimensional plot; (b) Young's moduli along the directions perpendicular to [001]; and (c) Young's moduli along the directions perpendicular [100] (from [11]).

Single crystal elastic parameters can also provide valuable insight into the characteristics of interatomic bonding through certain criteria, e.g. Cauchy's relationships, elastic anisotropy factors, Poisson's ratios, c_{33}/c_{11} ratio, etc. The Cauchy's relationships between the elastic stiffness constants for tetragonal crystals with central forces are [18]:

$$c_{13} = c_{44} \quad \text{and} \quad c_{12} = c_{66} \tag{3}$$

The data in Table 3 indicate that the Cauchy's relationships do not hold true for Mo_5Si_3 and this fact implies that the interatomic forces in Mo_5Si_3 are non-central. However, there is relatively less difference between c_{13} and c_{44} and between c_{12} and c_{66} for Mo_5Si_3 as compared with those of $C11_b$ and C40 transition metal disilicides [17], where the Cauchy's relationships do not hold true by more than a factor of 3 in some cases.

The elastic anisotropy factors of Mo_5Si_3 are tabulated in Table 4, along with those of $MoSi_2$. Table 4 suggests that the elastic anisotropy factors of Mo_5Si_3 are closer to unity than those of $MoSi_2$, although these factors still indicate that Mo_5Si_3 is anisotropic in elasticity.

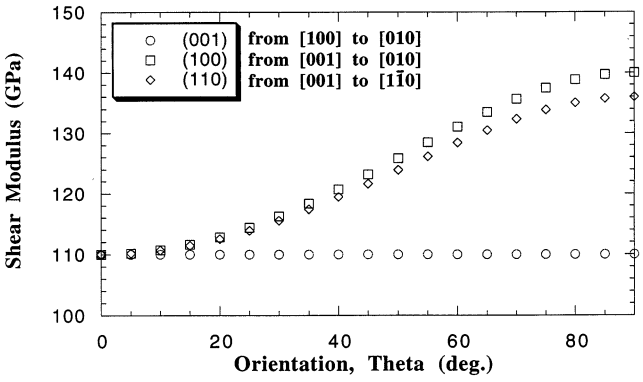

Fig. 2. Orientation dependence of the shear moduli of Mo_5Si_3 single crystals on the (001) plane from [110] to [010], the (100) plane from [001] to [010], and the (110) plane from [001] to [1$\bar{1}$0] (from [11]).

Table 4
Elastic anisotropy factors of Mo_5Si_3 and $MoSi_2$

Anisotropy factors	Mo_5Si_3	$MoSi_2$
c_{33}/c_{11}	0.874	1.255
c_{13}/c_{12}	0.804	0.796
$2c_{44}/(c_{11}-c_{12})$	0.809	1.401
$2c_{66}/(c_{11}-c_{12})$	1.029	1.345

The Poisson's ratios of Mo_5Si_3 are tabulated in Table 5, along with those of the $MoSi_2$. The data in Table 5 clearly demonstrate that the Poisson's ratios of Mo_5Si_3 single crystals are substantially larger than those of $MoSi_2$.

The c_{33} and c_{11} relationship of Mo_5Si_3 is different from that of $C11_b$ transition metal disilicides, e.g. $MoSi_2$ and WSi_2. For Mo_5Si_3, $c_{11} > c_{33}$ with $c_{33}/c_{11} = 0.87$. However, for $MoSi_2$ and WSi_2, $c_{33} > c_{11}$ with $c_{33}/c_{11} = 1.26$ [17]. This is related to the bonding strength along the [100] and [001] axes in the two intermetallic phases. As described above, the strongly bonded –Si–Mo–Si– chains are along [100] and [010] directions and the weakly bonded –Mo–Mo– and –Si–Si– chains are along [001] in Mo_5Si_3, therefore, c_{11} should be larger than c_{33} in this compound. On the other hand, the strongly bonded –Si–Mo–Si– chains are along [001] and the weakly bonded –Mo–Mo– and –Si–Si– chains are along [100] and [010] directions in $MoSi_2$ and WSi_2, therefore, c_{33} should be larger than c_{11} in these phases. Furthermore, Table 3 shows that $c_{11} + c_{12} > c_{33}$ for Mo_5Si_3. $c_{11} + c_{12} > c_{33}$ suggests that the elastic tensile modulus is larger on the (001) plane than along the [001] direction. This indicates that the bonding in the (001) plane is stronger than the bonding along the [001] direction for Mo_5Si_3. In fact, these results of bonding analysis in Mo_5Si_3 are consistent with the thermal expansion anisotropy ($\alpha_c/\alpha_a = 2.2$) of Mo_5Si_3. First-principles total energy and electronic structure calculations have confirmed these results, yielding more detailed information about interatomic bonding for Mo_5Si_3 [19].

The isotropic elastic moduli of Mo_5Si_3 can be derived by the Voigt, Reuss, or Hill approximation and compared with those of the constituent elements and the average values derived from the rule of mixtures. These values are given in Table 6. It can be seen that the isotropic elastic moduli and the Poisson's ratio of polycrystalline Mo_5Si_3 are close to those of Mo, especially the shear and Young's moduli. The rule of mixtures does not hold true for Mo_5Si_3. The Poisson's ratio of polycrystalline Mo_5Si_3 is 0.278 as shown in Table 6, which is substantially $> v \approx 0.15$ of the $C11_b$ transition metal disilicides and $v \approx 0.19$ of the C40 transition metal disilicides [17].

Table 5
The Poisson's ratios of Mo_5Si_3 and $MoSi_2$

Poisson's ratios	Mo_5Si_3	$MoSi_2$
$v_{31} = -s_{13}/s_{33}$	0.2255	0.1780
$v_{12} = -s_{12}/s_{11}$	0.3107	0.2570
$v_{13} = -s_{13}/s_{11}$	0.2464	0.1360

Table 6
The isotropic elastic moduli and Poisson's ratio of Mo_5Si_3. K is the bulk modulus, G the shear modulus, E the Young's modulus, and v the Poisson's ratio (from [11])

Materials	K (GPa)	G (GPa)	E (GPa)	v
Mo[a]	259.7	125.0	323.2	0.293
Si[a]	97.9	68.1	162.9	0.225
Mo_5Si_3: rule of mixture	199	104	263	0.268
Mo_5Si_3: Hill approximation	242	126	323	0.278

[a] compiled from the data in [20].

The specific Young's modulus (the ratio of the Young's modulus to the density of a material) is an important engineering design parameter for materials in aerospace applications. Fig. 3 demonstrates the specific Young's moduli of high temperature structural silicides. It can be seen from Fig. 3 that the specific Young's modulus of Mo_5Si_3 is, in general, smaller than those of transition metal disilicides but higher than those of nickel aluminides [25–32 GPa (g cm^{-3})$^{-1}$] and comparable with those of titanium aluminides [30–50 GPa (g cm^{-3})$^{-1}$].

3.3. Residual thermal stress

Fig. 4 shows the residual thermal stress due to a spherical grain of Mo_5Si_3 in an infinite matrix of Mo_5Si_3 with a misorientation such that the thermal expansion mismatch is maximized. It can be seen that

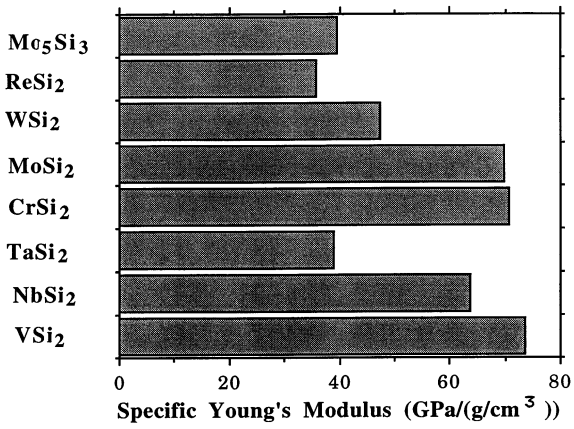

Fig. 3. Specific Young's modulus of high temperature structural silicides.

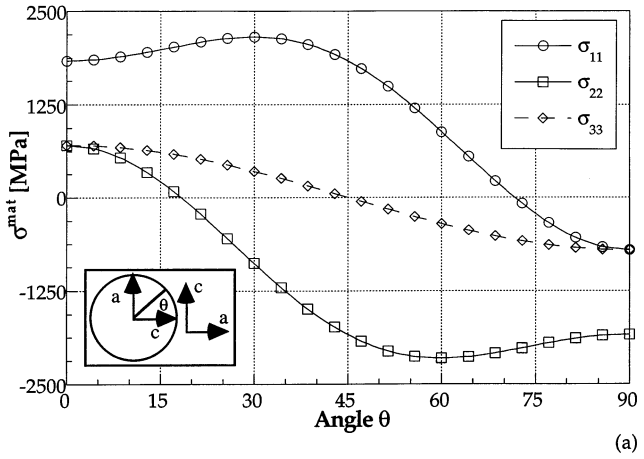

$$\sigma^{grain} = \begin{pmatrix} 1840 & 0 & 0 \\ 0 & -1840 & 0 \\ 0 & 0 & 0 \end{pmatrix} \text{[MPa]} \quad \text{(b)}$$

Fig. 4. Stresses for a spherical grain of Mo_5Si_3 embedded in an infinite matrix of Mo_5Si_3 misoriented such that the thermal expansion mismatch is maximized. (a) matrix; (b) grain.

the tensile stress in the Mo_5Si_3 matrix can reach a maximum of about 1.8 GPa during the cooling from the melting point.

In the calculation of the residual thermal stress next to a planar interface of two Mo_5Si_3 grains, the stress is calculated as a function of misorientation of the two grains characterized by θ_1 and θ_2, as shown in Fig. 5. Fig. 6 demonstrates that a maximum of up to 1 GPa thermal stress can develop near a planar interface of two grains with certain misorientation in Mo_5Si_3.

Although it is not practical to calculate the residual thermal stresses for all possible cases, the two calculations for the two typical cases clearly demonstrate that a substantially high residual thermal stresses, up to 1.8

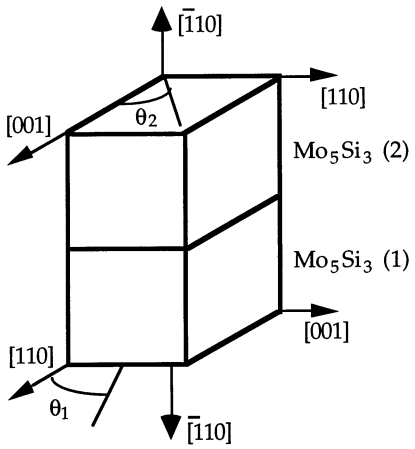

Fig. 5. Initial crystallography and rotation scheme to calculate residual thermal stresses in a planar interface as a function of misorientation.

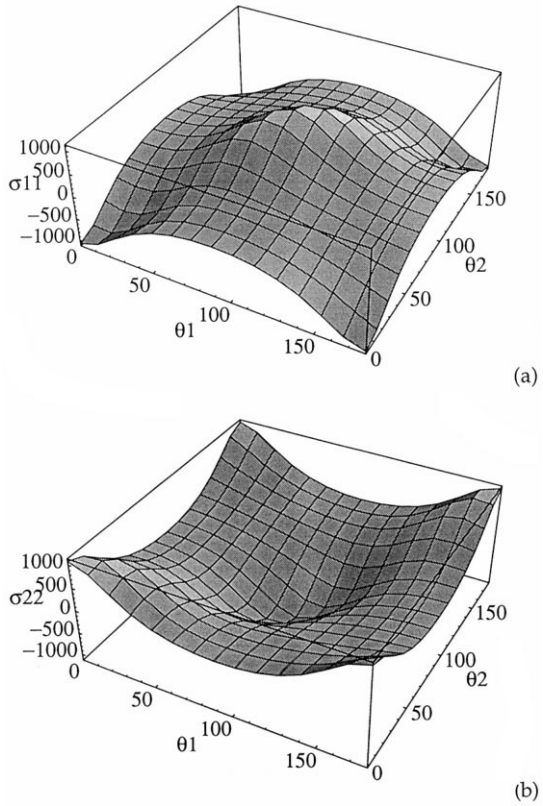

Fig. 6. Thermal stresses (in MPa) for a planar interface shown in Fig. 5 as a function of the misorientation. (a) σ_{11}; (b) σ_{22}.

GPa, can develop in Mo_5Si_3 due to thermal expansion mismatch between different grains. These large stresses, which are obviously higher than the compression and tension strength, can fracture weakly bonded grain boundaries in cooling processes during fabrication, unless other mechanisms to relieve these stresses are operative, such as dislocation plasticity, twinning formation, stress induced phase transformation, etc. Indeed, significant grain boundary cracking was observed in the arc-melted buttons and rods used in this study. Therefore, the Mo_5Si_3-based materials can only be properly studied and/or applied using: (a) single crystals; (b) polycrystals with very small grain sizes; or (c) Mo_5Si_3 properly alloyed by some elements, e.g. boron, to avoid the grain boundary cracking problem [21,22].

3.4. Mechanical behavior

The orientation dependence of the room temperature Vickers hardness, calculated from Eq. (1), on the (100) and (001) planes of Mo_5Si_3 single crystals is shown in Fig. 7(a). The hardness on these planes of Mo_5Si_3 is not significantly orientation dependent and the hardness has large values around 1200 kg mm^{-2}, which are substantially higher than those of $MoSi_2$ single crystals (600–900 kg mm^{-2}, depending on the testing orientations) [23] and those of $NbSi_2$ single crystals ($\approx$ 700 kg

mm^{-2}, depending on the testing orientations) [24]. It is interesting to note that there is a noticeable difference ($\approx 10\%$) between the hardness on the same (001) plane but with different indenter diagonal orientations.

Fig. 7(b) demonstrates the orientation dependence of the indentation fracture toughness, roughly estimated from Eq. (2), on the (100) and (001) planes of Mo_5Si_3 single crystals. It can be seen from Fig. 7(b) that the room temperature indentation fracture toughness on these planes of Mo_5Si_3 is 2–2.5 $MPa\sqrt{m}$, showing a minor orientation dependence. These values are comparable to those of $MoSi_2$ single crystals in some orientations [23]. It is also interesting to note that there is a noticeable difference ($\approx 10\%$) between the fracture toughness on the same (001) plane but with different indenter diagonal orientations.

SEM micrographs of the indentation impressions and the associated cracks on the (100) and (001) planes with two indenter diagonal orientations are shown in Fig. 8. Dislocation slip traces are not observed near the indent impressions, suggesting that dislocation slip may not be operative for these mechanical loading at ambient temperature in Mo_5Si_3. Fig. 8 also demonstrates that the cracks are generated at the four corners of the indent impression and no secondary cracks are observed for Mo_5Si_3. On the other hand, cracks may be generated at only two corners of some indent impressions and substantial secondary cracks are observed for $MoSi_2$ [23]. Therefore, the fracture behavior of Mo_5Si_3 may be less anisotropic than that of $MoSi_2$. The significant feature is that the indentation shapes for the two different indenter diagonal orientations on the (001) plane are completely different, as shown in Fig. 8(c) and (d). This may be responsible for the noticeable differences ($\approx$ 10%) in the hardness and fracture toughness for these indentations as mentioned above. It is important to understand the reason(s) why such a significant difference exists in the plastic response to the same loading by considering the elastic properties and examining the plastic deformation mechanisms in Mo_5Si_3. Studies are underway to evaluate this phenomenon.

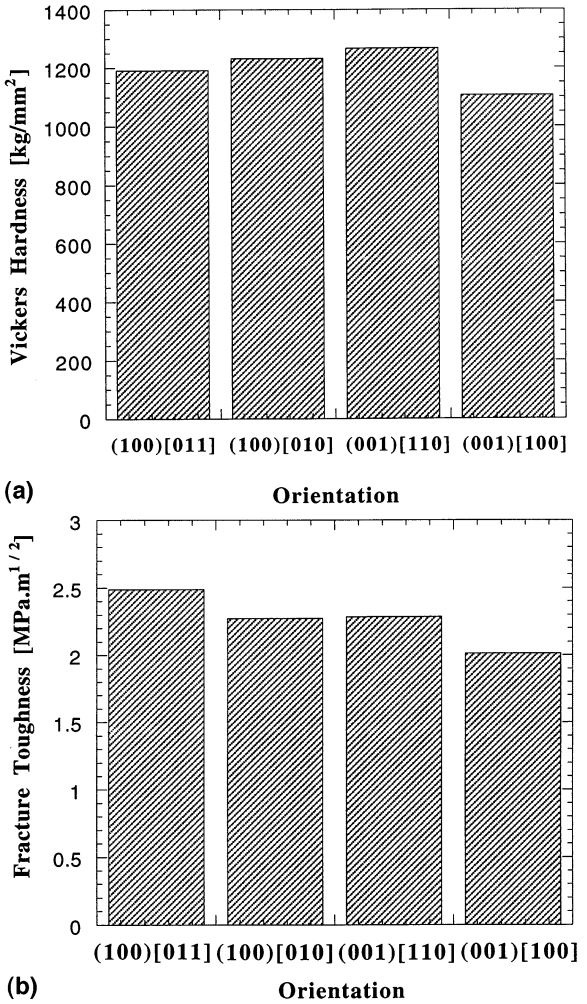

Fig. 7. The orientation dependence of (a) the room temperature Vicker's hardness and (b) the indentation fracture toughness on the (100) and (001) planes of Mo_5Si_3 single crystals. (100)[011] means the indentation is on the (100) plane and one indenter edge is parallel to [011] (from [11]).

4. Conclusions

The physical properties and mechanical behavior of Mo_5Si_3 single crystals have been studied. Four primary conclusions have been reached:

1. Mo_5Si_3 single crystals with minimal oxygen and nitrogen impurities (≈ 10 wppm) have been synthesized by both the optical floating zone and the Czochralski methods. Silicon loss in alloy processing and single crystal growth is < 0.5 at.%.
2. Thermal and elastic properties of Mo_5Si_3 single crystals have been experimentally measured. Mo_5Si_3 has the CTEs of $\alpha_a = 5.2 \times 10^{-6}\ °C^{-1}$ and $\alpha_c = 11.5 \times 10^{-6}\ °C^{-1}$, showing a strong thermal expansion anisotropy ($\alpha_c/\alpha_a = 2.2$). Mo_5Si_3 has room temperature single crystal elastic constants of $c_{11} = 446$, $c_{33} = 390$, $c_{13} = 140$, $c_{12} = 174$, $c_{44} = 110$, and $c_{66} = 140$ GPa, respectively. Analysis of the elastic parameters reveals that the bonding in the (001) plane is stronger than the bonding along the [001] direction and the crystal anharmonicity is higher along the [001] direction for Mo_5Si_3.
3. Significantly large residual thermal stresses (up to 1.8 GPa) can develop in Mo_5Si_3 in the solidification process due to thermal mismatch between different grains, causing grain boundary cracking.
4. Room temperature Vickers indentation tests on the (100) and (001) planes reveal that Mo_5Si_3 have a hardness of around 1200 kg mm^{-2} and a fracture toughness above 2 $MPa\sqrt{m}$. Plastic responses (the shape of indent impression) to the (001) indenta-

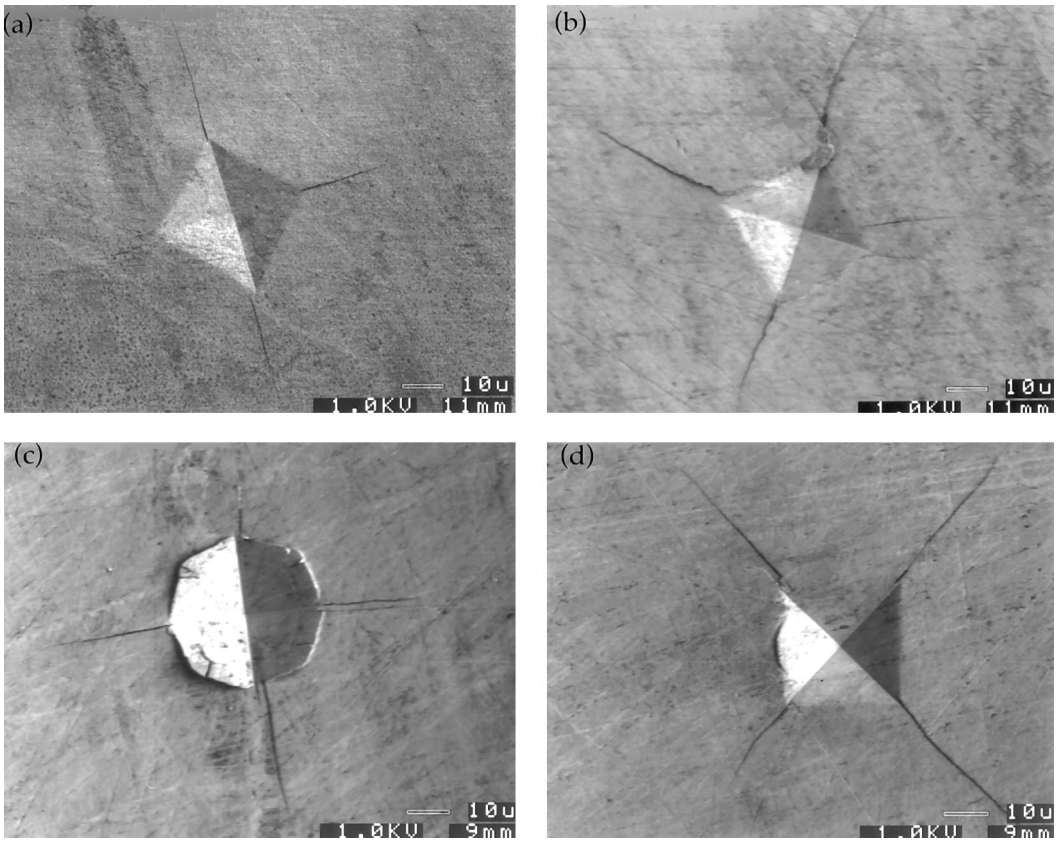

Fig. 8. SEM micrographs of the indentation impressions and the associated cracks on Mo_5Si_3 single crystals: (a) on the (100) plane with one indenter edge parallel to [011]; (b) on the (100) plane with one indenter edge parallel to [010]; (c) on the (001) plane with one indenter edge parallel to [110]; and (d) on the (001) plane with one indenter edge parallel to [100] (from [11]).

tions with two different indenter diagonal orientations are significantly different, resulting in a noticeable difference in the corresponding hardness and fracture toughness.

Acknowledgements

This work has been supported by the US Department of Energy, Basic Energy Sciences (Division of Materials Science).

References

[1] J.J. Petrovic, MRS Bull. XVIII (1993) 35.
[2] T.B. Massalski, (Ed.), Binary Alloy Phase Diagram, ASM, Pittsburgh, 1986, p. 2666.
[3] A.K. Vasudevan, J.J. Petrovic, Mat. Sci. Eng. A155 (1992) 1.
[4] D.M. Shah, D. Berczik, D.L. Anton, R. Hecht, Mat. Sci. Eng. A155 (1992) 45.
[5] R. Gibala, H. Chang, C. Czarnik, K. Edwards, A. Misra, in: J.J. Darolia, C.T. Lewandowski, P.L. Liu, D.B. Martin, DO AGAINMiracle, and M. V. Nathal Structural Intermetallics, TMS, Warrendale, PA, 1993, 561.
[6] M. Yamaguchi, H. Inui, in: R. Darolia, J.J. Lewandowski, C.T. Liu, P.L. Martin, D.B. Miracle, M.V. Nathal (Eds.), Structural Intermetallics, TMS, Warrendale, PA, 1993, p. 127.
[7] Y. Umakoshi, T. Nakashima, T. Nakano, E. Yanagisawa, MRS Symp. Proc. 322 (1994) 9.
[8] S.A. Maloy, T.E. Mitchell, A.H. Hauer, Acta Metall. Mater. 43 (1995) 657.
[9] M.K. Meyer, M. Akinc, J. Am. Ceram. Soc. 79 (1996) 938.
[10] M.K. Meyer, M.J. Kramer, M. Akinc, Intermetallics 4 (1996) 273.
[11] F. Chu, D.J. Thoma, K.J. McClellan, P. Peralta, Y. He, Intermetallics (1998) (in press).
[12] J.D. Eshelby, Proc. Roy. Soc. Lond. A241 (1957) 376.
[13] R.J. Asaro, D.M. Barnett, J. Mech. Phys. Solids 23 (1975) 77.
[14] P. Peralta, T.E. Mitchell, to be submitted to Scripta Mater. (1998).
[15] G.R. Anstis, P. Chantyikul, B.R. Lawn, D.B. Marshall, J. Am. Ceram. Soc. 64 (1981) 533.
[16] Y. He, R.B. Schwarz, A. Migliori, S.H. Whang, J. Mater. Res. 10 (1995) 1187.
[17] F. Chu, Ming Lei, S.A. Maloy, J.J. Petrovic, T.E. Mitchell, Acta Mater. 44 (1996) 3035.
[18] J.F. Nye, Physical Properties of Crystals, Oxford University Press, London, UK, 1979.
[19] C.L. Fu, Xindong Wang, Y.Y. He, K.M. Ho, Intermetallics (1998) (in press).
[20] G. Simmons, H. Wang, Single Crystal Elastic Constants and Calculated Aggregate Properties: A Handbook, The M.I.T. Press, Cambridge, MA, 1971.

[21] D.M. Berczik, R.J. Hecht, private communications.
[22] C.T. Liu, J. Schneibel, M.H. Yoo, private communications.
[23] P. Peralta, S.A. Maloy, F. Chu, J.J. Petrovic, T.E. Mitchell, Scripta Mater. 37 (1997) 1599.
[24] S.A. Maloy, F. Chu, J.J. Petrovic, T.E. Mitchell, in: W.O. Soboyejo, H.L. Fraser, T.S. Srivatsan (Eds.), Deformation and Fracture of Ordered Intermetallic Materials 111, TMS, Warrendale, PA, 1996.